mtFociCounter: Quantitative and open source single-cell analysis of mitochondrial nucleoids and other foci.

Timo Rey[1] , Michal Minczuk[1]

[1] MRC Mitochondrial Biology Unit, Cambridge University, Cambridge UK
ORCID, TR: 0000-0002-2124-937X, MM: 0000-0001-8242-1420

Abstract:

The circular, multi-copy genome of mammalian mitochondria (mtDNA) is tightly regulated at the cellular level. The exact mechanisms by which mtDNA copy number homeostasis is achieved in health and disease however, remains largely elusive. Current real-time PCR and next generation sequencing technologies can only estimate average copy numbers from bulk samples, albeit single-cell approaches are emerging. On contrary, microscopy analysis of mtDNA-related foci allow not only to assess average copy numbers, but also their heterogeneity at the single cell level, as well as to preserve spatial context. We developed *mtFociCounter*, a reproducible, open source, free image analysis pipeline to quantify mitochondrial foci from single cells. *mtFociCounter* has a modular architecture, allowing single cell segmentation, foci counting and optional foci filtering and contextualisation in a transparent and reproducible manner. It provides a simple, all-in-one approach for (semi-)automated foci quantification. Gateways for integration of specialised image segmentation software are provided, while ensuring a unified and comparable output. We applied *mtFociCounter* to wild-type 3t3 mouse fibroblasts and found large cell-to-cell heterogeneity of the number of nucleoids, mitochondrial area and nucleoid density across over 480 cells. Our results raise concerns about the use of bulk-sample approaches to study mitochondrial nucleoid homeostasis, as well as provide a ready-to-use solution to this problem. In the near future, we will apply *mtFociCounter* to study different sample conditions to better understand mitochondrial DNA homeostasis, as well as further develop the *mtFociCounter*. For this, we are actively looking for feedback and suggestions, and are happy to assist in efforts to test the current version of *mtFociCounter* in other laboratories.

Introduction:

Mitochondria are dynamic cellular organelles which occur in a vast range of forms and shapes, depending on the type and state of their host cell (Tilokani *et al*, 2018). To build the oxidative phosphorylation (OXPHOS) apparatus, crucial for cellular energy production, mitochondria express their own genome (mtDNA). Human and mouse mtDNA is circular, encodes 37 essential genes within ~16.6kb and is stored as small (~100nm) granules, termed nucleoids (Brown *et al*, 2011; Kukat *et al*, 2011). Upon transcription, mitochondrial RNA condensates into transient, fluid granules of similar size, which are called Mitochondrial RNA Granules (MRGs) (Iborra *et al*, 2004; Antonicka & Shoubridge, 2015; Jourdain *et al*, 2016; Rey *et al*, 2020) (see **Fig.1a**). The amount of mtDNA is tightly regulated at the cellular level and ranges from 100 to 100'000 copies depending on cell type and cell state (Stewart & Chinnery, 2015; D'Erchia *et al*, 2015; Filograna *et al*, 2020; Sasaki *et al*, 2017). Aberrations of mtDNA copy-number control are associated with several primary mitochondrial disorders and common diseases including cancer, cardiovascular disease and neurodegeneration (Castellani *et al*, 2020; Filograna *et al*, 2019, 2020; Zeviani & Viscomi, 2022). While mtDNA compaction or transcription regulation by TFAM likely plays a role, the complete mechanism by which cells regulate mtDNA homeostasis is not well understood (Kanki *et al*, 2004; Filograna *et al*, 2019). Reliable determination of the copy-number of mtDNA in a specimen, therefore, is not only important for fundamental biomedical and cell-biological research but also for diagnostics.

In addition to their number, nucleoids within a cell can differ in a variety of other factors, such as the probability to replicate or the amount of protein that is associated with a specific focus (Brüser *et al*, 2021). For mitochondrial transcription and MRGs on the other hand, the degree and importance of cellular homeostasis and the existence of subspecies is yet to be explored.

To determine the number of mtDNA molecules per cell, current methods rely on quantitative PCR and sequencing (Filograna *et al*, 2020). Hereby, mtDNA content from bulk samples can be normalised to nuclear DNA abundance to obtain per-cell estimates. However, these methods do not preserve any information beyond the averaged number and sequence of mtDNA molecules from bulk samples, and do not allow to assess the variability between cells. While novel single-cell sequencing methods are emerging, they are only on the virtue of sensitivity to capture mtDNA (Lareau *et al*, 2021). A recent alternative method to quantify mtDNA copy number from single cells by droplet digital PCR holds greater promise, but is currently limited in throughput and lacks spatial information (O'Hara *et al*, 2019; Burr & Chinnery, 2022). However, mtDNA-molecule number alone, without insight on their spatial distribution, is not a reliable marker for mitochondrial states ((Ban-Ishihara *et al*, 2013)), and similar considerations apply to mtRNAs.

Both, nucleoids and MRGs can be visualised by fluorescence microscopy and, due to their size below the diffraction limit, form distinctive foci on microscopy images (see **Fig.1b-d**). Single mammalian cells can contain 1'000s of nucleoids and by counting mitochondrial foci on fluorescence images it is possible to estimate this number within live or fixed cells. Determining mitochondrial foci-

number by microscopy bears several advantages over sequencing based approaches. First, it preserves spatial information and local or relative concentration differences can be assessed with subcellular or suborganellar resolution. Different sub-types of foci can therefore be quantified (Brüser *et al*, 2021). In addition, quantitative methods for image analysis developed for one foci-type are readily transferable to other types, allowing direct comparison, for instance between one nucleoid marker and another. However, to quantify large datasets of microscopy images to achieve statistically relevant sampling can be daunting. Manual approaches, which are still applied today, are therefore often limited to few 10s of cells and 100s of foci for subsequent analysis (Xavier & Martinou, 2021; Silva-Pinheiro *et al*, 2021). However, sample heterogeneity and human factors make it very difficult to quantify large datasets in consistent and reproducible ways (see **Fig.1c**). Automation of foci-counting on the other hand readily allows scaling to 100s of cells and 10'000s of foci (Kukat *et al*, 2011; Kotrys *et al*, 2021; Brüser *et al*, 2021). In addition, automated analysis drastically reduces random errors and observer biases and allows, in principle, to perfectly trace and reproduce the experimental workflow from raw images to final results.
Unfortunately, the majority of currently used automated approaches for mitochondrial foci quantification use commercial software and closed source code (Kukat *et al*, 2011; Kotrys *et al*, 2021; Brüser *et al*, 2021). The choice of influential parameters is not communicated and together, the reproduction of previously published results, therefore, is hardly possible. Furthermore, the transferability of these approaches between laboratories is very low and comparison of results or sequential studies across groups and projects is extremely difficult.

Figure 1: Mitochondrial DNA and RNA foci. **a)** Schematic of the central dogma within mitochondria. mtDNA is organised into fluid condensates termed nucleoids (magenta). mtRNA is transcribed as long, polycistronic precursors and accumulates in fluid droplets, Mitochondrial RNA Granules or MRGs (green). Upon processing, mitochondrial mRNA is translated into OXPHOS-complex subunits, which produce ATP via a proton-gradient. **b)** Spinning disk confocal image of 3t3 mouse cells with nucleoids stained with anti-DNA antibody (magenta), mitochondria highlighted by mitochondrially targeted dsRed. (yellow) and DAPI-stained nuclei (cyan). **c)** Enlarged inlets from **b** as indicated by Roman numbers with nucleoids in magenta and mitochondria in grey-scale. Defining what is an individual focus by eye is often ambiguous, depends on visualisation settings and is hardly reproducible. **d)** Confocal image of U2OS human cells MRGs stained by anti-BrU antibody (green) after 60min of BrU-incubation and mitochondria stained by anti-tom20 antibody (blue).

In this work, we created an easy-to-use, free and open source software tool to quantify mitochondrial or other cellular foci with single-cell resolution. To this end, we present a Fiji-plugin (Schindelin *et al*, 2012), which we call mitochondrial foci counter, or *mtFociCounter*. allowing users a simple approach to (semi-)automatically quantify microscopy images from a vast range of imaging modalities, from standard Widefield and Confocal to superresolution microscopes. mtFociCounter returns the number of foci per cell and several other, optional descriptors. All metadata to fully trace and reproduce every step from raw image to final results is preserved. Furthermore, it is readily downloadable as open source code, from Github (https://github.com/TimoHenry). Its modular design, the open source code and the integration in the well established framework of Fiji also allows to continuously improve and update mtFociCounter in the future. This means users can adapt and add parts of the software to meet their specific needs while preserving a uniform and comparable output format. We exemplify the use of *mtFociCounter* by assessing the reproducibility of nucleoid quantification and cell-to-cell heterogeneity in 3t3 mouse fibroblasts.

Results:

mtFociCounter design and architecture

mtFociCounter is a Fiji-plugin which currently comprises three modules: *ToTiff*, *CellOutline* and *FociCounter* (see **Fig.2**). Each module can be run independently, and is discussed briefly in the following.
The *ToTiff* module converts raw microscopy images into a standard Tiff-file format with a few clicks (see **Fig.2b** and **Suppl.Fig.2a**). The user is asked to choose a directory containing all input files, and a new folder will be created to contain only .tiff files. Hereby, the original file-extension (or ending) serves as a flag to find input-images. If images are already available in Tiff format, the *ToTiff* module can be skipped.
The *CellOutline* module then takes Tiff-image files as input and allows to segment individual cells (see **Fig.2c**). For this, 3D raw-images are maximum-intensity projected and all colours combined into a single, 2D image. The user is then asked to manually outline individual cells with a simple brush-tool. This step allows to manually curate the input-data. For instance, dead or heavily overlapping cells, which could not be segmented with high confidence, can be excluded. The coordinates of every region-of-interest (ROI) of manually segmented cells are saved and allow to reproduce this step. Then, a cropped image is created and saved for every segmented cell for further processing. If preferred, cells can be singled out by other software, and directly processed by the *FociCounter* module described below. To assist with cell segmentation, Wheat Germ Agglutinin (WGA) staining can be used (ThermoFischer: W11261). However, we

found that WGA does not allow confident separation of medium densely cultured 3t3 fibroblast cells (see **Suppl.Fig.2d**). Instead, the *CellCatcher* module of the recently published *MitoHacker* workflow (Rohani *et al*, 2020) may represent a viable alternative for mitochondria-channel based cell segmentation.

To quantify the number of foci per cell, the *FociCounter* module provides several options. The basic input requirement are 2D Tiff images containing a ROI, which includes one cell (see **Suppl.Fig.2b**). The user is then asked to specify which channel contains the foci to analyse. *FociCounter* uses the built-in *FindMaxima* function from Fiji to detect foci. For this, a prominence value needs to be set, which influences the number and type of foci detected. *FociCounter* encourages the user to perform a parameter sweep of six prominence values and requires to define a range of values. This allows to monitor the effect of the parameter-settings and to reduce parameter-bias (see **Fig.3a**). Depending on the input images, the optimal prominence value can range from 10 - 100'000au, and needs to be optimised for a given experimental set-up. The detected foci are both output as a binary images as well as a list of ROIs. With the ROIs, it is possible to visually assess the quality of detected foci depending on the prominence, when overlaid onto the corresponding single cells image. To by-pass the sweep, the same number can be entered for the beginning and end of the range. *FociCounter* also provides the option to use other channels from multicolour images to automatically curate the detected foci. To ensure only mitochondrial foci are detected, mitochondria images can be used to create a mask and to filter the foci by enabling the "Filter with mitochondria" option. While a manual segmentation option is provided, it is not recommended to use it for medium to high-throughput analysis. Instead, a simple automated approach based on Fiji's *Convert To Mask* works well for clean images (see **Suppl.Fig.2c**). A machine-learning based approach to segment mitochondria is not yet implemented into mtFociCounter, but choosing the option: "pre-segmented" provides an easy gateway to use specialised software such as Ilastik (Berg *et al*, 2019) or Weka (Arganda-Carreras *et al*, 2017) for this often difficult task to accurately segment mitochondria. In addition to foci-filtering, the area of the mitochondria within each cell is measured from the binary mask. This can serve as an approximation for cell size, as the mitochondrial content is difficult to dissociate from cell size (Kitami *et al*, 2012). It is evident that other fluorescent images, for instance staining organelles such as the ER, can also be used to filter foci by co-localisation. To filter by exclusion, the option: "Subtract nucleus" can be ticked. Because the antibody against mtDNA not only detects mitochondrial nucleoids but also has many targets in the nucleus (see **Suppl.Fig. 2g**), this is a useful feature to count only mitochondrial foci. The same options for "pre-segmented", "automated" and "manual" segmentation are available, while a "learning-based" option awaits implementation. For automated segmentation, a nuclear staining such as DAPI is required. However, for manual segmentation it can be possible to re-use mitochondria, as the nuclear shape is often detectable by eye (see **Suppl.Fig.2a**). The segmented features for exclusion or inclusion are saved as binary files for every cell, and can be used for further quantification as well as to ensure traceability and reproducibility of the full analysis pipeline (see **Suppl.Fig. 2c**).

Together, the modular design of mtFociCounter provides a simple, adaptable Fiji-plugin to quantify cellular foci. In addition to semi- and fully automated options for coherent and reproducible quantification of mitochondrial foci, it readily allows to integrate other specialised software, and to be adapted to different questions. Below, we will exemplify its use by quantifying the number and density of mtDNA-nucleoids in single 3t3 mouse fibroblast cells.

Figure 2: **Workflow of mtFociCounter**. **a)** First, a user chooses one of the modules to process their data. Each module is run individually, depending on the available input data. **b)** The *ToTiff*-module converts various image-file type to TIFF images, which can subsequently be used as input. **c)** To segment single cells from tiff images, the *CellOutline*-module can be used, providing different options. **d)** Next, foci are detected using a range of prominence values defined by the user. Optionally, foci counted from the nuclear (or other) area can then be excluded while mitochondria (or other) channels can be used to create an inclusion filter. **e)** Finally, a python script as a jupyter notebook produces publication-ready figures as shown in **Fig.3**. Example images of intermediary output for each module are shown in **Suppl.Fig2**.

mtDNA foci distribution in wild-type fibroblasts

To test the mtFociCounter we quantified the number of mitochondrial nucleoids per single cell in cultured NIH 3t3 mouse fibroblasts. To this end, we created a stable cell line expressing mitochondrially targeted dsRed, (MTS-dsRed), using the SU9-targeting sequence as previously described (Gäbelein *et al*, 2022). Cells were then fixed, and nucleoids stained with antibodies against mtDNA. The nucleus was stained with DAPI and three-colour fluorescence images were acquired on a standard spinning disk confocal microscope (see **Fig.1b**). Next, we used the *ToTiff* module to convert raw images from *.ims to *.tiff format (see **Fig.2b**). We created z-projected composite images based on maximum intensity values and manually segmented individual cells using the *CellOutline* module (see **Fig.2c** and **Suppl.Fig.2a & b**). Dividing cells with insufficiently separated nuclei and cytosols or with condensed chromosomes, as well as cells with faint mitochondrial signal were not included (see **Suppl.Fig.2e & f**). In total, we analysed 481 single 3t3 wild-type (WT) fibroblasts from three biological replicates of cells, which were seeded on different days, and originated from two separate batches of thawed cells. With the *FociCounter* module, we then tested a range of prominence values in a parameter-sweep between 5 and 200 au (**Fig.3a**) and between 5 and 50 (data not shown). Raw foci-binary images (see **Suppl.Fig.2g**) were first filtered using mitochondrial (see

Suppl.Fig.2h) and nuclear (see **Suppl.Fig.2i**) binary masks before quantification. For this, we used the *FociCounter* module to automatically segment mitochondria with a simple threshold. We manually segmented nuclei using the DAPI-channel to exclude mtDNA-foci which are detected within the nuclear area. Automated segmentation of nuclei also works, but depends on a consistently bright DAPI-staining. Filtered foci-binaries were then turned into ROIs, which were counted and can be visualised by overlay (see **Fig.2c**).

In agreement with visual inspection, we observed a sharp drop of detected foci at low prominence values, indicating a clear difference between real positive and false positive signals (see **Fig.3a**). We decided to fix the prominence level at 122 au for further analysis (see **Fig.3b**). We observed a mean number of 322 per single cell, with a standard deviation of +/-135 foci (n=481 cells). However, the number of detected foci per cell is not normally distributed ($p=1*10^{-12}$, see **Suppl.Fig.3a**), and we found a median number of 302 foci. Using the mitochondria mask, the mitochondrial area was recorded by *FociCounter* for every single cell (see **Fig.3b**). We then computed the mean mitochondrial area per cell to be 237.43 μm^2 with a standard deviation of +/-105.76 μm^2 (n=481 cells). Again, the distribution of mitochondrial area does not follow a Normal distribution ($p=7*10^{-16}$, see **Suppl.Fig.3b**) and the median mitochondrial area observed was 216.69 μm^2. The wide distribution of values for both, number of foci and mitochondrial area is exemplified by the very large standard deviations. The coefficient of variation for foci per cell was 42% and 44.5% for the mitochondrial area, and the interquartile ranges (IQR) were 193 and 125.69 μm^2 for the number of foci and mitochondrial area respectively.

Next, we assessed whether foci-number and mitochondrial area are correlated within single cells. Indeed, we found that the number of foci per cell is strongly correlated with the mitochondrial area of that same cell (Corr=0.87, n=481 cells, see **Fig.3c**). This is in accordance with the literature, which found a semi-regulated spacing of nucleoids along mitochondria across eukaryotic species (Lewis *et al*, 2016; Jajoo *et al*, 2016), as well as our own observations of a positive correlation between MRGs and mitochondrial length (Rey *et al*, 2020), both suggesting a link between total mitochondrial area of a cell and foci number.

To distinguish between potential effects on cell size and thus mitochondrial network-size, and mitochondrial foci number such as number of nucleoids, we propose to normalise foci-counts by mitochondrial area. Upon normalisation, we found a mean nucleoid-density of 1.388 foci/μm^2 and a standard deviation of +/-0.247 (n=481 cells, see **Fig.3b**). The distribution of nucleoid-density is much closer to Normal, with few outliers for very small mitochondria (p=0.00098, see **Suppl.Fig.3c**). Interestingly, when extreme data-points below 0.75 foci/μm^2 are excluded, the distribution is not significantly different from a Normal distribution (data not shown). The median number of foci/μm^2 is 1.401, the coefficient of variation 17.8% and the IQR is 0.305.

To assess the sampling effect and reproducibility of our sample preparation procedure, we compared the data from three biological replicates (see **Fig.3d**). The number of foci per cell were significantly different between the three replicates (Shannon-Wilcoxon-U-test, alpha = 1%). Interestingly, the mitochondrial area between the first replicate (20220603, n=163) and the third replicate (20220708, n=213) were not differentiable, whereas the second replicate (20220706, n=105) was different from both. Notably, the foci-density differs less between the different biological replicates, albeit the second replicate is clearly different from the third (see **Fig.3d**).

We also investigated the variability between technical replicates of samples which were processed in parallel, whereby seeding, fixing, staining and image-acquisition was performed simultaneously for all samples (see **Suppl.Fig.3d**). Unfortunately, this reduces the sample-size to less than 100 cells per sample. Where per-sample sample-sizes were highest, on replicate one (n=76 and n=87), we found no statistical significance between technical replicates, indicating that our sample-preparation procedure is reproducible. However, for the other two biological replicates, the large cell-to-cell heterogeneity and low number of samples between n=41 and n=88 resulted in significant differences between, in principle, technically identical samples.

In addition to our results described above, we also acquired datasets of 3t3 fibroblasts with a point-scanning confocal, and a super-resolution Elyra7 SIM^2 microscope, as well as using an anti-tom20 antibody instead of MTS-dsRFP expression, for mitochondrial staining (see **Suppl.Fig.3e and f**). The image acquisition on these microscopes has a much lower throughput, inherent to the microscopy technique (point-scanning) or FOV and post-processing (SIM^2). In return, both allow to increase the resolution by fine-tuning the acquisition parameters and thereby provide higher accuracy, in particular for mitochondria. We observed that staining mitochondria by tom20-antibody considerably increases the noise, and we recommend using fluorescent proteins for organelle segmentation whenever possible. Together, our data exemplifies the straight forward transferability of the mtFociCounter-approach to different microscopy techniques, depending on the availability and desired emphasis between accuracy and throughput.

Figure 3: Mitochondrial nucleoid analysis in 3t3 wild-type cells with mtFociCounter. a) Number of foci counted per cell for n=481 cells from three pooled biological replicates with differing prominence values. **b)** Kernel density estimates and histograms of foci (magenta, left), mitochondrial area (yellow, centre) and normalised foci density (pink, right) with a fixed prominence value of 122 au from all cells analysed in **a**. **c)** Scatter plot of foci-count and mitochondrial area for every cell with regression-fit (blue line) and standard deviation (shaded). Histograms of the distribution of the number of detected mtDNA-foci (y-axis, right) and mitochondrial area (x-axis, top) are shown. A good positive correlation between foci-count and mitochondrial area was found (R=0.87). **d)** Comparison of biological replicates for foci count (left, magenta), mitochondrial area (centre, yellow) and foci density (right, pink) are shown as box plots. Number

of cells for each biological replicate (sampled on different days) comprises two or three technical replicates (sampled and treated in parallel), and are indicated below the plots. All box plots show the first and third quartiles and the median, whiskers comprise the rest of the distributions except outliers. Where applicable, a two-tailed Mann-Whitney U-test was performed, and **** denotes p-values < 0.0001, 'ns' denotes non-significant differences (alpha = 5%) and all data-points are shown as purple dots.

Discussion:

To understand the biological processes that underlie the regulation of mitochondrial gene expression in health and disease, it remains crucial to improve reproducibility and availability of tools for mitochondrial foci quantification by (semi-)automated image analysis (see **Fig.1**). We created a user-friendly, free and open source software to quantify mitochondrial foci as a Fiji-plugin, *mtFociCounter*. It has a modular design and readily allows users to fine-tune and adapt the workflow to their experimental set-up (see **Fig.2**). It also provides gateways to use other, specialised software for segmentation, while producing generalised and comparable output data. We exemplify the quantitative analysis of mitochondrial nucleoids by *mtFociCounter* in mouse fibroblasts and showcase the use of a transparent parameter-sweep (see **Fig.3a**). In 3t3 fibroblasts we find a large variability between individual WT cells (see **Fig.3b**). This is in good agreement with recent reports of single cell mtDNA copy-numbers (O'Hara *et al*, 2019; Burr & Chinnery, 2022), and large heterogeneity between individual cells is expected (Symmons & Raj, 2016). Furthermore, in mixed populations of proliferative cells, such as most cultured cell lines, cellular state occupation does not necessarily follow a Normal distribution. It is therefore not surprising that we do not find the number of nucleoids or the mitochondrial area to be normally distributed across individual cells (see **Fig.3b**). However, this raises concerns about the meaningfulness of bulk-sample average (mean) measurements of the number of mtDNA-molecules per cell, as a readout of mtDNA-homeostasis. The correlation between nucleoid number and mitochondrial mass, which we observe, further implies that differences in cell growth or mitochondrial biogenesis cannot readily be distinguished from effects on nucleoid homeostasis by determining the number of mtDNA molecules per cell (see **Fig.3c**). We therefore propose to normalise mitochondrial nucleoid counts by mitochondrial mass, mitochondrial area or other measures of cell size. The here reported mean and median occupancy of nucleoids along the mitochondrial network is on the same order as for MRGs (Rey *et al*, 2020). Interestingly, in our experiments, nucleoid-densities still do not follow a Normal distribution, albeit further sampling could help to rule out that the remaining deviation is not due to confounding measurement errors from few small cells with clustered mitochondria (see **Suppl.Fig.2h**).

In addition, the large cell-to-cell variability creates challenges when sampling single cells at low throughput. We found that experimental replicates can differ significantly for small sample sizes below or around n=100 (see **Fig.3**, **Suppl.Fig.3**). We therefore propose to sample at least one to two hundred cells per technical replicate. Depending on the methods for sample preparation, such as immunostaining of mitochondria (see **Suppl.Fig.3e**), we further propose that that Control and Treated samples are processed in parallel, to avoid confounding batch-effects.

Limitations and outlook

The presented beta-version of *mtFociCounter* has some remaining short-comings, and will be further improved in the near future. One of the current limitations for higher throughput applications is the need for manual segmentation to isolate single cells reliably. Required user input may restrict the transferability from one laboratory to another, albeit the implementation of *CellOutline* allows to trace decisions on previously analysed data, and thereby perfect reproducibility. In addition, pre-segmented cells can already be used as input, providing a gateway for combination with other software. In the future, alternative, automated cell-segmentation strategies will be assessed and directly implemented into *mtFociCounter* to enhance ease-of-use. Novel Machine Learning approaches for nuclear and mitochondrial segmentation could also provide useful additions. A second limitation can be the raw-data analysis, which is currently based on openly available python code. The development of a simpler user-interface will enhance the accessibility to researchers without any programming skills, albeit the data can already be analysed by other means.

It is important to note that a fully reproducible analysis pipeline does not guarantee fully reproducible results. Prior to comparative assays, it is crucial to optimise the sample preparation using control cells. *mtFociCounter* allows to compare technical replicates and thereby quantify the reproducibility of a particular experimental setup (see **Suppl.Fig.3**). We found that low sampling frequency impairs reproducibility due to the large cell-to-cell heterogeneity. For truly conclusive verification of our experimental setup we will therefore increase the sampling to at least one or two hundred cells per independent replicate. However, high quality plus high-resolution microscopy still represents the major bottleneck for high throughput mitochondrial analysis.

Finally, the possibility to quantify of other cellular characteristics, such as cell cycle state, foci state or correlation between different foci would provide useful additions to the *mtFociCounter* in the future. Therefore, we look forward to comments, input and contributions to further improve and adapt this platform for a wider range of applications, increased throughput and further improved data quality.

Conclusion:

Here, we provide a platform to concentrate low and medium through-put efforts to quantitatively analyse effects on mitochondrial health, *mtFociCounter*. We demonstrate the use of *mtFociCounter* to analyse single cell variability of mitochondrial nucleoid density in mouse fibroblasts as well as the reproducibility of our experimental design and required sampling frequency. *mtFociCounter* represents a framework to study effects on mitochondrial foci number in a quantitative and reproducible manner, as well as allowing to assess cell-to-cell heterogeneity of foci numbers and densities beyond mitochondria. This allows to overcome current limitations to accurately determine the effect of treatments or mutations on mitochondria, based on bulk-measurements.

Material and methods:

Cell culture

Cells were grown in growth medium with DMEM GlutaMax (Gibco: 31966-021) supplemented with 1% PenStrep and 10% Calf Serum (ATCC: 30-2030). Calf Serum instead of Fetal Calf Serum is used to maintain proliferative cell populations of NIH/3t3 fibroblasts (ATCC: CRL-1658^{TM}). Stable cell-lines expressing MTS-dsRed were created as previously described (Gäbelein *et al*, 2022). In brief, wild-type or mutant cells were transformed with lentivirus to express MTS-dsRed. Cells were then FACS-sorted for high expression of dsRed and subsequently preserved in cryo-stocks or cultured for no more than 20 passages, to ensure genetic coherence across experiments.

Immunofluorescence

Cells were seeded on 12 mm glass slide cover slips (epredia: CB00130RAC20MNZ0) in different wells of 24-well plates, and at a density of 50'000 cells per well. The next day, the medium was aspirated and 300 µL of pre-warmed 4% PFA (Thermo scientific: J19943-K2) was added for 20 min of fixation at room temperature (RT). Samples were then rinsed once, and washed with PBS two times for 10 min at RT. Optionally, samples were refrigerated (4 °C) for some hours at this step, before continued processing later on the same day. The cells were then permeabilised for 10-20 min with 250uL of 0.1% Triton X-100 (Fluka: 93420), before blocking with 300 µL of 5% BSA (Sigma: A7030-100G) in PBS for 15-30 min at RT. For immunostaining, anti-mtDNA antibodies (EMD Millipore: CBL186) and anti-tom20 antibodies (Proteintech: 11802-1-AP) were then diluted in 5% BSA at a ratio of 1:250 (a solution of at least 125 µL was made to reduce pipetting errors), and cover slips were flipped onto 20 µL drops of antibody-solution on parafilm for 1 hour of incubation in a humid chamber at RT. Samples were then rinsed once and washed two times for 5-15 min with PBS. Next, anti-IgM Alexa 647 antibodies (Invitrogen: A21238) were diluted in 5% BSA at a ratio of 1:750 (a solution of at least 350 µL was made) and cover slips incubated as described above, for 45 min. Cover slips were then flipped onto drops of DAPI diluted in PBS (1:5000) and incubated for 15 min before again rinsing and washing in PBS. Individual cover slips were then mounted onto a drop of ProLong Gold (Invitrogen: P10144) and cured at 4 °C over night, in a dark but ventilated chamber. Samples were always imaged the next day, to avoid sample deterioration.

Microscopy

The qualitative example image of MRGs in U2OS cells was taken on a SP8-STED in regular Confocal mode (see **Suppl.Fig.1c**). **Suppl.Fig.2d** was acquired on a Zeiss LSM880 point scanning confocal microscope with Zen software, using a Plan-Apochromat 63x/1.40 Oil DIC M27 objective. 405, 488, 561 and 633nm laser lines and adequate filter settings were used to sequentially acquire each channel for minimal bleed-through. All other images were acquired using an Andor Dragonfly 500 confocal spinning disk system on a Nikon Eclipse TiE inverted microscope. Image stacks were taken at 0.3 µm intervals, and using a 100x or 60x objective lense (NA1.4). We used 405 nm, 561 nm or 633 nm excitation lasers and acquired images on a Zyla 4.2 PLUS sCMOS camera with Fusion software (Andor).

Image Analysis

All image processing and analysis was done using the mtFociCounter workflow described in this article and the complete source code is available on Github. We set the prominence range for our images between 5 and 200 au. We used the manual segmentation option for the nuclei using the DAPI-channel as input, because the DAPI-signal was too low for rigorous automation but good for visual determination of the nuclear shape. Mitochondria were automatically detected, and used to filter the foci, as well as to determine the cell area. Raw-data was then processed with python 3, using a jupyter notebook which is also available on Github.

Software

Only free and open-source software was used for this project, with the exception of microscope-steering, as indicated, and microsoft power point for figure arrangement. For analysis, MiniConda was used as a package manager to run python 3 and jupyter notebooks. For writing, reference management and image-generation, LibreOffice, Zotero and Fiji were used respectively.

Accessibility:

All data and code are freely accessible on the data-repository Zenodo (doi: 1.5281/zenodo.6962215) and Github (https://github.com/TimoHenry) respectively. Please do not hesitate to contact the authors in case of unclarity, questions about the use, suggestions for improvements or any other queries. Please make changes to the source code and submit improvements via Github. Biological material may be available upon reasonable request.

Acknowledgments:

This research was funded by EMBO Long Term Fellowship 2021-152. We thank Pedro Pinheiro-Silva for 3t3 NIH cell lines, Christoph Gäbelein and Julia Vorholt for stable cell line creation, Benoît Kornmann and Quian Feng for plasmids, and Suliana Manley for the support during the initial conceptualisation.

Competing interests:

Michal Minczuk is co-founder and scientific advisor at Pretzel Therapeutics Inc. Beyond this, the authors do not declare any competing interests.

References:

Antonicka H & Shoubridge EA (2015) Mitochondrial RNA Granules Are Centers for Posttranscriptional RNA Processing and Ribosome Biogenesis. *Cell Reports* 10: 920–932

Arganda-Carreras I, Kaynig V, Rueden C, Eliceiri KW, Schindelin J, Cardona A & Sebastian Seung H (2017) Trainable Weka Segmentation: a machine learning tool for microscopy pixel classification. *Bioinformatics* 33: 2424–2426

Ban-Ishihara R, Ishihara T, Sasaki N, Mihara K & Ishihara N (2013) Dynamics of nucleoid structure regulated by mitochondrial fission contributes to cristae reformation and release of cytochrome c. *Proceedings of the National Academy of Sciences* 110: 11863–11868

Berg S, Kutra D, Kroeger T, Straehle CN, Kausler BX, Haubold C, Schiegg M, Ales J, Beier T, Rudy M, *et al* (2019) ilastik: interactive machine learning for (bio)image analysis. *Nat Methods* 16: 1226–1232

Brown TA, Tkachuk AN, Shtengel G, Kopek BG, Bogenhagen DF, Hess HF & Clayton DA (2011) Superresolution Fluorescence Imaging of Mitochondrial Nucleoids Reveals Their Spatial Range, Limits, and Membrane Interaction. *Molecular and Cellular Biology* 31: 4994–5010

Brüser C, Keller-Findeisen J & Jakobs S (2021) The TFAM-to-mtDNA ratio defines inner-cellular nucleoid populations with distinct activity levels. *Cell Reports* 37: 110000

Burr SP & Chinnery PF (2022) Measuring Single-Cell Mitochondrial DNA Copy Number and Heteroplasmy using Digital Droplet Polymerase Chain Reaction. *JoVE*: 63870

Castellani CA, Longchamps RJ, Sun J, Guallar E & Arking DE (2020) Thinking outside the nucleus: Mitochondrial DNA copy number in health and disease. *Mitochondrion* 53: 214–223

D'Erchia AM, Atlante A, Gadaleta G, Pavesi G, Chiara M, De Virgilio C, Manzari C, Mastropasqua F, Prazzoli GM, Picardi E, *et al* (2015) Tissue-specific mtDNA abundance from exome data and its correlation with mitochondrial transcription, mass and respiratory activity. *Mitochondrion* 20: 13–21

Filograna R, Koolmeister C, Upadhyay M, Pajak A, Clemente P, Wibom R, Simard ML, Wredenberg A, Freyer C, Stewart JB, *et al* (2019) Modulation of mtDNA copy number ameliorates the pathological consequences of a heteroplasmic mtDNA mutation in the mouse. *Sci Adv* 5: eaav9824

Filograna R, Mennuni M, Alsina D & Larsson N (2020) Mitochondrial DNA copy number in human disease: the more the better? *FEBS Lett*: 1873-3468.14021

Gäbelein CG, Feng Q, Sarajlic E, Zambelli T, Guillaume-Gentil O, Kornmann B & Vorholt JA (2022) Mitochondria transplantation between living cells. *PLOS Biology* 20: e3001576

Iborra FJ, Kimura H & Cook PR (2004) The functional organization of mitochondrial genomes in human cells. *BMC Biology* 2

Jajoo R, Jung Y, Huh D, Viana MP, Rafelski SM, Springer M & Paulsson J (2016) Accurate concentration control of mitochondria and nucleoids. *Science* 351: 169–172

Jourdain AA, Boehm E, Maundrell K & Martinou J (2016) Mitochondrial RNA granules: Compartmentalizing mitochondrial gene expression. *J Cell Biol* 212: 611–614

Kanki T, Ohgaki K, Gaspari M, Gustafsson CM, Fukuoh A, Sasaki N, Hamasaki N & Kang D (2004) Architectural Role of Mitochondrial Transcription Factor A in Maintenance of Human Mitochondrial DNA. *Mol Cell Biol* 24: 9823–9834

Kitami T, Logan DJ, Negri J, Hasaka T, Tolliday NJ, Carpenter AE, Spiegelman BM & Mootha VK (2012) A Chemical Screen Probing the Relationship between Mitochondrial Content and Cell Size. *PLoS ONE* 7: e33755

Kotrys AV, Borowski LS & Szczesny RJ (2021) High-Throughput Measurement of Mitochondrial RNA Turnover in Human Cultured Cells. In *Mitochondrial Gene Expression*, Minczuk M & Rorbach J (eds) pp 133–146. New York, NY: Springer US

Kukat C, Wurm CA, Spahr H, Falkenberg M, Larsson N-G & Jakobs S (2011) Super-resolution microscopy reveals that mammalian mitochondrial nucleoids have a uniform size and frequently contain a single copy of mtDNA. *Proceedings of the National Academy of Sciences* 108: 13534–13539

Lareau CA, Ludwig LS, Muus C, Gohil SH, Zhao T, Chiang Z, Pelka K, Verboon JM, Luo W, Christian E, *et al* (2021) Massively parallel single-cell mitochondrial DNA genotyping and chromatin profiling. *Nat Biotechnol* 39: 451–461

Lewis SC, Uchiyama LF & Nunnari J (2016) ER-mitochondria contacts couple mtDNA synthesis with mitochondrial division in human cells. *Science* 353: aaf5549

O'Hara R, Tedone E, Ludlow A, Huang E, Arosio B, Mari D & Shay JW (2019) Quantitative mitochondrial DNA copy number determination using droplet digital PCR with single-cell resolution. *Genome Res* 29: 1878–1888

Rey T, Zaganelli S, Cuillery E, Vartholomaiou E, Croisier M, Martinou J-C & Manley S (2020) Mitochondrial RNA granules are fluid condensates positioned by membrane dynamics. *Nat Cell Biol* 22: 1180–1186

Rohani A, Kashatus JA, Sessions DT, Sharmin S & Kashatus DF (2020) Mito Hacker: a set of tools to enable high-throughput analysis of mitochondrial network morphology. *Sci Rep* 10: 18941

Sasaki T, Sato Y, Higashiyama T & Sasaki N (2017) Live imaging reveals the dynamics and regulation of mitochondrial nucleoids during the cell cycle in Fucci2-HeLa cells. *Sci Rep* 7: 11257

Schindelin J, Arganda-Carreras I, Frise E, Kaynig V, Longair M, Pietzsch T, Preibisch S, Rueden C, Saalfeld S, Schmid B, *et al* (2012) Fiji: an open-source platform for biological-image analysis. *Nat Methods* 9: 676–682

Silva-Pinheiro P, Pardo-Hernández C, Reyes A, Tilokani L, Mishra A, Cerutti R, Li S, Rozsivalova D-H, Valenzuela S, Dogan SA, *et al* (2021) DNA polymerase gamma mutations that impair holoenzyme stability cause catalytic subunit depletion. *Nucleic Acids Research* 49: 5230–5248

Stewart JB & Chinnery PF (2015) The dynamics of mitochondrial DNA heteroplasmy: implications for human health and disease. *Nat Rev Genet* 16: 530–542

Symmons O & Raj A (2016) What's Luck Got to Do with It: Single Cells, Multiple Fates, and Biological Nondeterminism. *Molecular Cell* 62: 788–802

Tilokani L, Nagashima S, Paupe V & Prudent J (2018) Mitochondrial dynamics: overview of molecular mechanisms. *Essays in Biochemistry* 62: 341–360

Xavier VJ & Martinou J-C (2021) Visualization of Mitochondrial RNA Granules in Cultured Cells Using 5-Bromouridine Labeling. In *Mitochondrial Gene Expression*, Minczuk M & Rorbach J (eds) pp 69–73. New York, NY: Springer US

Zeviani M & Viscomi C (2022) Mitochondrial Neurodegeneration. *Cells* 11: 637

Figure 1

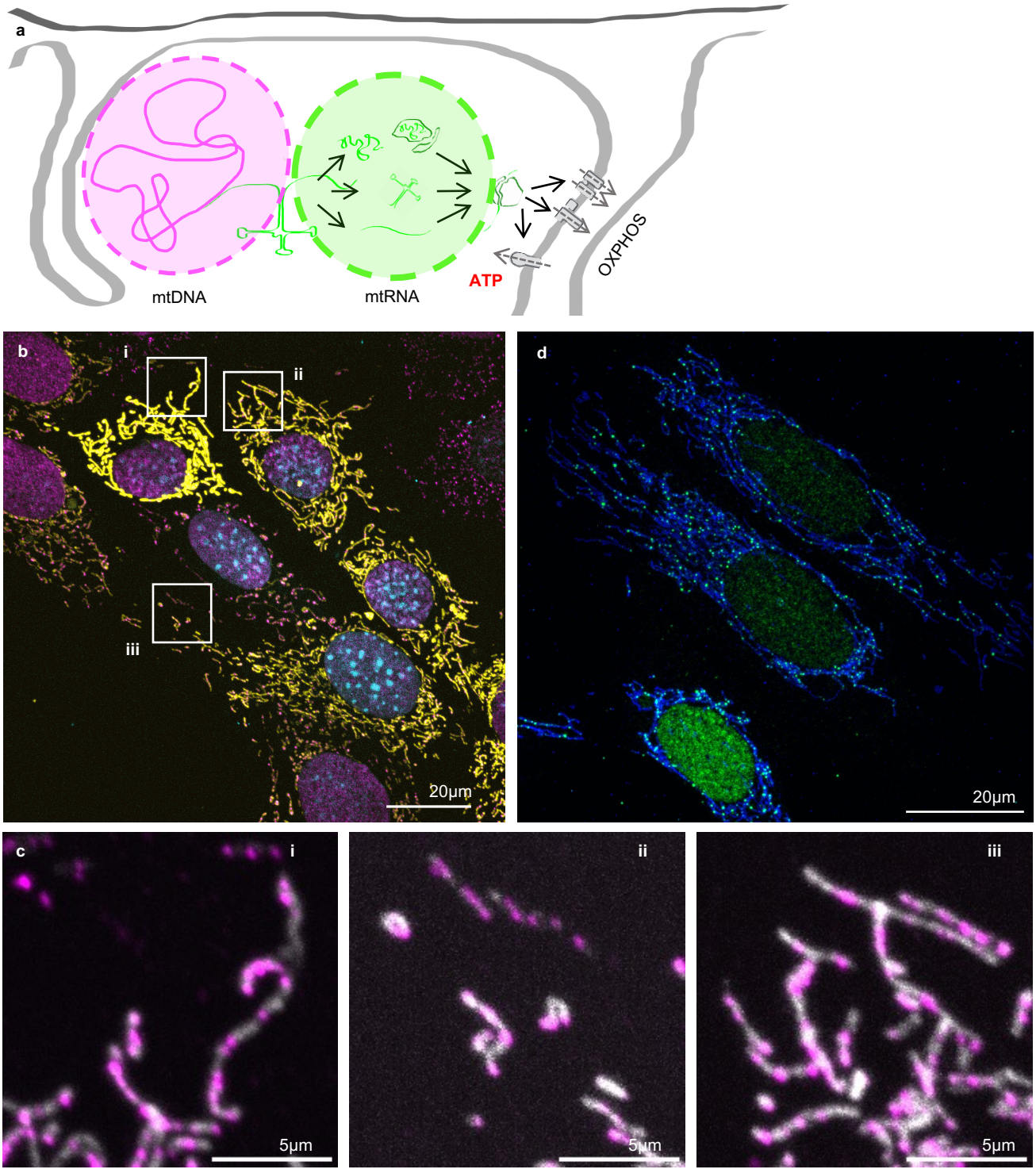
a
mtDNA
mtRNA
ATP
OXPHOS
b
i
ii
iii
20μm
d
20μm
c
i
5μm
ii
5μm
iii
5μm

Figure 2

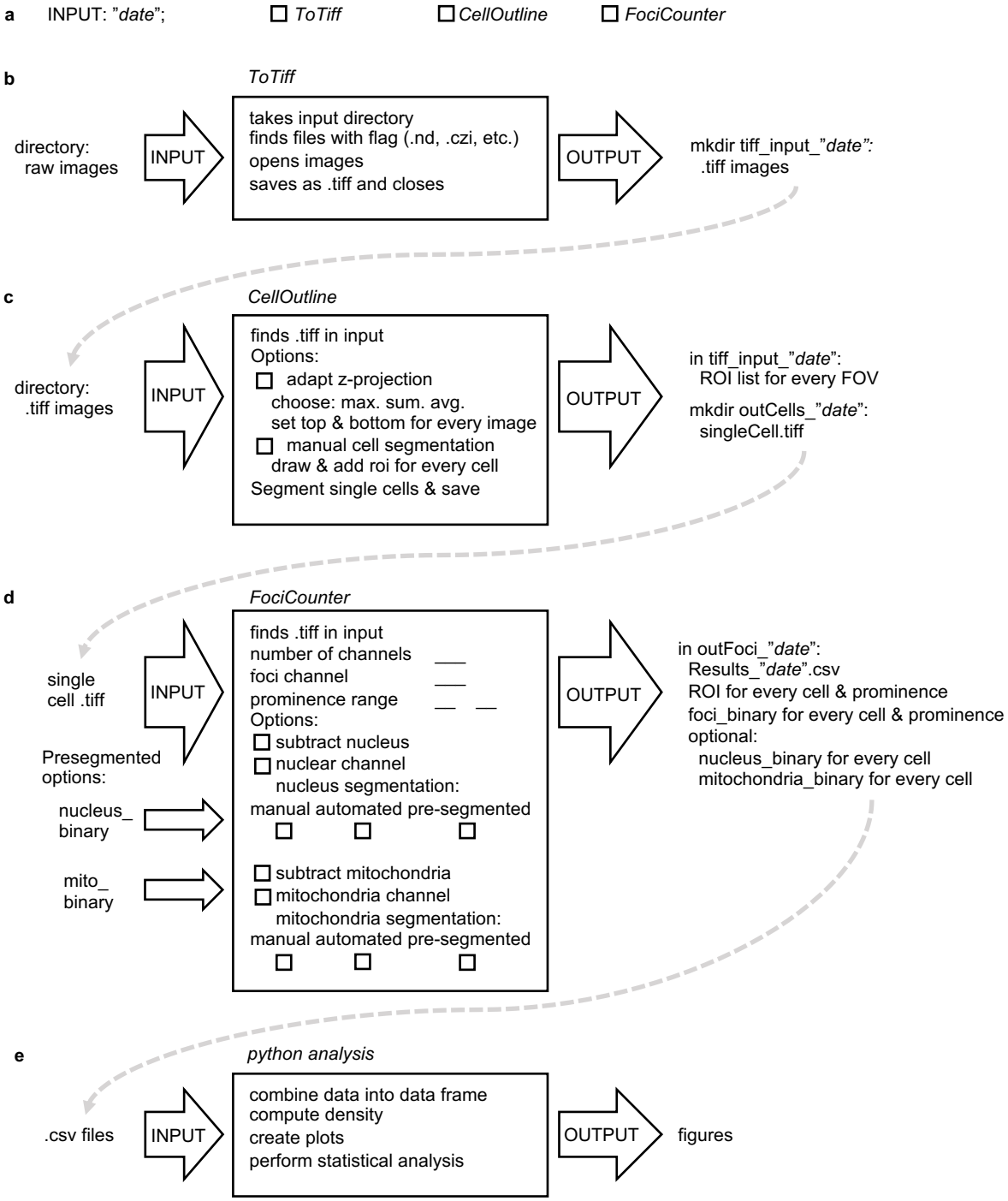
a
INPUT: "date";
ToTiff
CellOutline
FociCounter
b
ToTiff
directory:
raw images
INPUT
takes input directory
finds files with flag (.nd, .czi, etc.)
opens images
saves as .tiff and closes
OUTPUT
mkdir tiff_input_"date":
.tiff images
c
CellOutline
directory:
.tiff images
INPUT
finds .tiff in input
Options:
adapt z-projection
choose: max. sum. avg.
set top & bottom for every image
manual cell segmentation
draw & add roi for every cell
Segment single cells & save
OUTPUT
in tiff_input_"date":
ROI list for every FOV
mkdir outCells_"date":
singleCell.tiff
d
FociCounter
single
cell .tiff
INPUT
finds .tiff in input
number of channels
foci channel
prominence range
Options:
subtract nucleus
nuclear channel
nucleus segmentation:
manual automated pre-segmented
Presegmented
options:
nucleus_
binary
mito_
binary
subtract mitochondria
mitochondria channel
mitochondria segmentation:
manual automated pre-segmented
OUTPUT
in outFoci_"date":
Results_"date".csv
ROI for every cell & prominence
foci_binary for every cell & prominence
optional:
nucleus_binary for every cell
mitochondria_binary for every cell
e
python analysis
.csv files
INPUT
combine data into data frame
compute density
create plots
perform statistical analysis
OUTPUT
figures

Figure 3

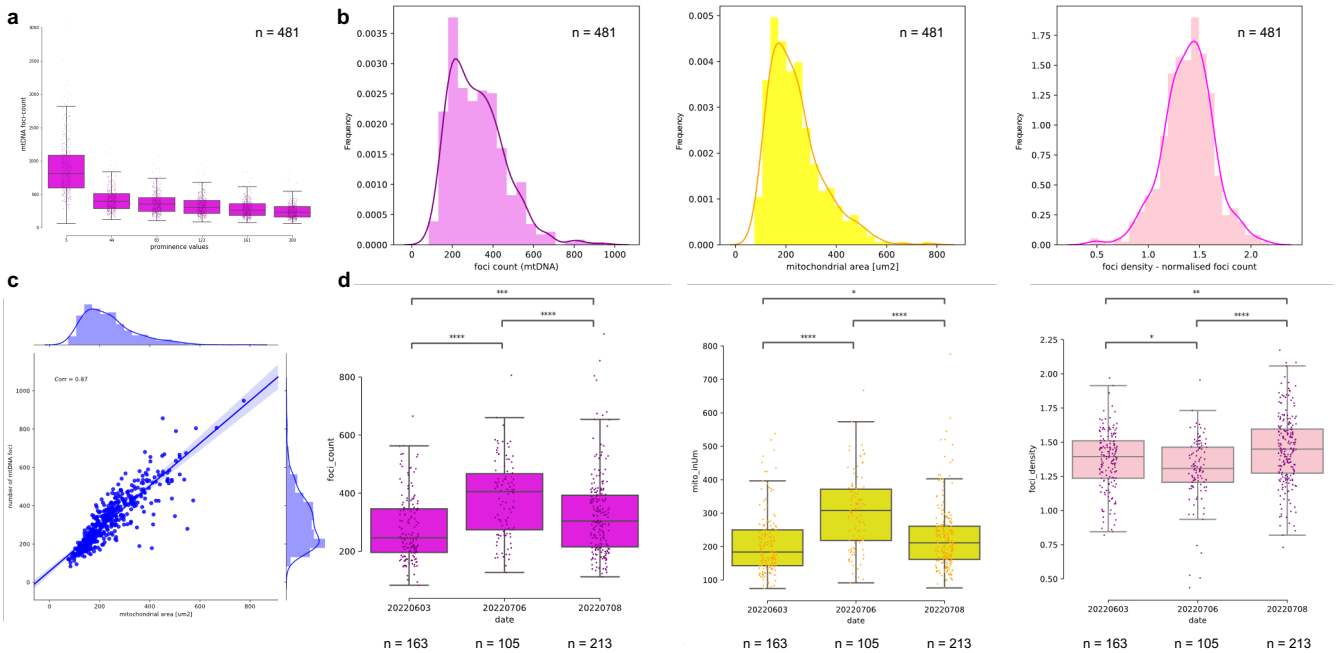
a
n = 481
mtDNA foci count
prominence values
b
n = 481
Frequency
foci count (mtDNA)
n = 481
Frequency
mitochondrial area [um2]
n = 481
Frequency
foci density - normalised foci count
c
Corr = 0.87
number of mtDNA foci
mitochondrial area [um2]
d
foci_count
mito_inUm
foci_density
20220603
20220706
20220708
date
n = 163
n = 105
n = 213

Supplementary Figures:

Supplementary Figure 1, Mitochondrial DNA and RNA foci.

a) Left, three colour composite confocal image of 3t3 fibroblasts stably expressing MTS-dsRed (yellow), stained with antibodies against mtDNA and with Alexa 647 (magenta), and DAPI (cyan). Centre and right, individual channels of the same FOV.

b) Left, two colour composite confocal image of U2OS cells after 60 min of BrU incubation, stained with antibodies against tom20 (blue) and BrU (green), and with Alexa 488 and Alexa 647 respectively. Centre and right, individual channels of the same FOV.

Supplementary Figure 2, Workflow of the mitoFociCounter.

a) An example image with multiple cells is shown. The cell-to-cell variability in shape, size and expression levels is apparent. Mitochondria are stained in yellow (MTS-dsRed), nucleus in cyan (DAPI) and nucleoids in magenta (anti-mtDNA Alexa647). The image is a projection of the maximum intensity for each pixel across several z-planes.

b) A single cell from **(a)** outlined by manually drawn ROI (yellow dash), as output by the *CellOutline* module.

c) Example output from the *FociCounter* module with nucleus and mitochondria options, analysing the cell from **(b)**. Top two rows: binary images of detected foci for each prominence parameter: 5, 44, 83, 122, 161, 200 (from top left to bottom right). Bottom row, left: binary of manually segmented nucleus; centre: binary of automatically generated mitochondrial mask; right: overlay of final, counted ROIs (prominence: 122) on composite image with mtDNA (magenta) & mitochondria (blue) channels.

d) Example image of maximum intensity projected point scanning confocal image of maximum inten

e) and **f)** Example images of other FOVs, with arrows pointing to actively dividing cells.

g - i) Montages of all binaries produced and used to quantify sample 2 from replicate 20220603. g**)** Shows all foci detected using prominence level of 122. **h)** Contains all mitochondrial masks used to filter foci. i**)** With nuclear masks used to filter nuclear signal.

Supplementary Figure 3, Mitochondrial nucleoid analysis in 3t3 wild-type cells with mitoFociCounter.

a) - c) Quantile-Quantile plots indicating that foci count **(a)**, mitochondrial area **(b)** and foci density **(c)** do not follow a normal distribution. Notably it is mostly the smallest and largest values which do not follow the expected trend, and foci density, in particular, is very close to normal.

d) Box plots which denote the first and third quartiles and the median and whiskers comprising the rest of the foci density distributions are shown for each biological and technical replicate. Left, all data of 3t3 wild-type cells are shown in side-by side comparison, with number of analysed single cells indicated. Then, individual technical replicates of sample slides which were processed and images in parallel are compared side-by-side for the sampling days: 20220603, 20220706, 20220708. Two-tailed Mann-Whitney U-test were performed, and **** denotes p-values < 0.001, *** denotes p-values < 0.001, ** denotes p-values < 0.01, * denotes p-values < 0.05 and 'ns' denotes non-significant differences (alpha = 5%) and all data-points are shown as purple dots.

e) Single FOV of 3t3 WT fibroblasts, with mitochondria in blue (MTS-dsRed) and nucleoids in magenta (anti-mtDNA Alexa647), as imaged with LSM880 Point Scanning Confocal microscope. Left: overlay of both channels, centre: mitochondria only, right: foci only.

f) Single FOV of a 3t3 WT fibroblast, with mitochondria in blue (MTS-dsRed) and nucleoids in magenta (anti-mtDNA Alexa647), as imaged with Elyra7 SIM^2. Left: overlay of both channels, centre: mitochondria only, right: foci only.

Supplementary Figure 1

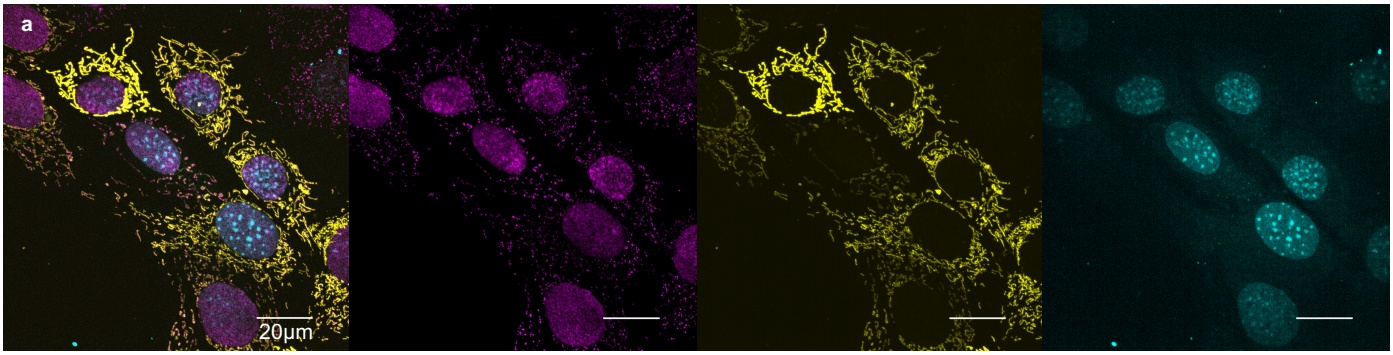

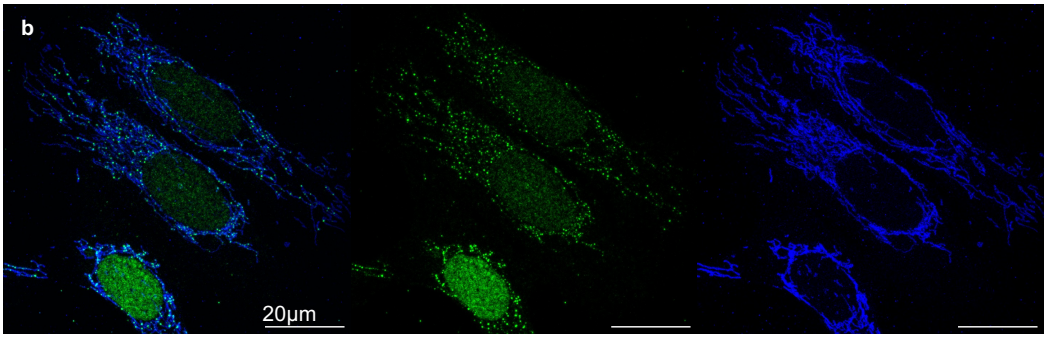

Supplementary Figure 2

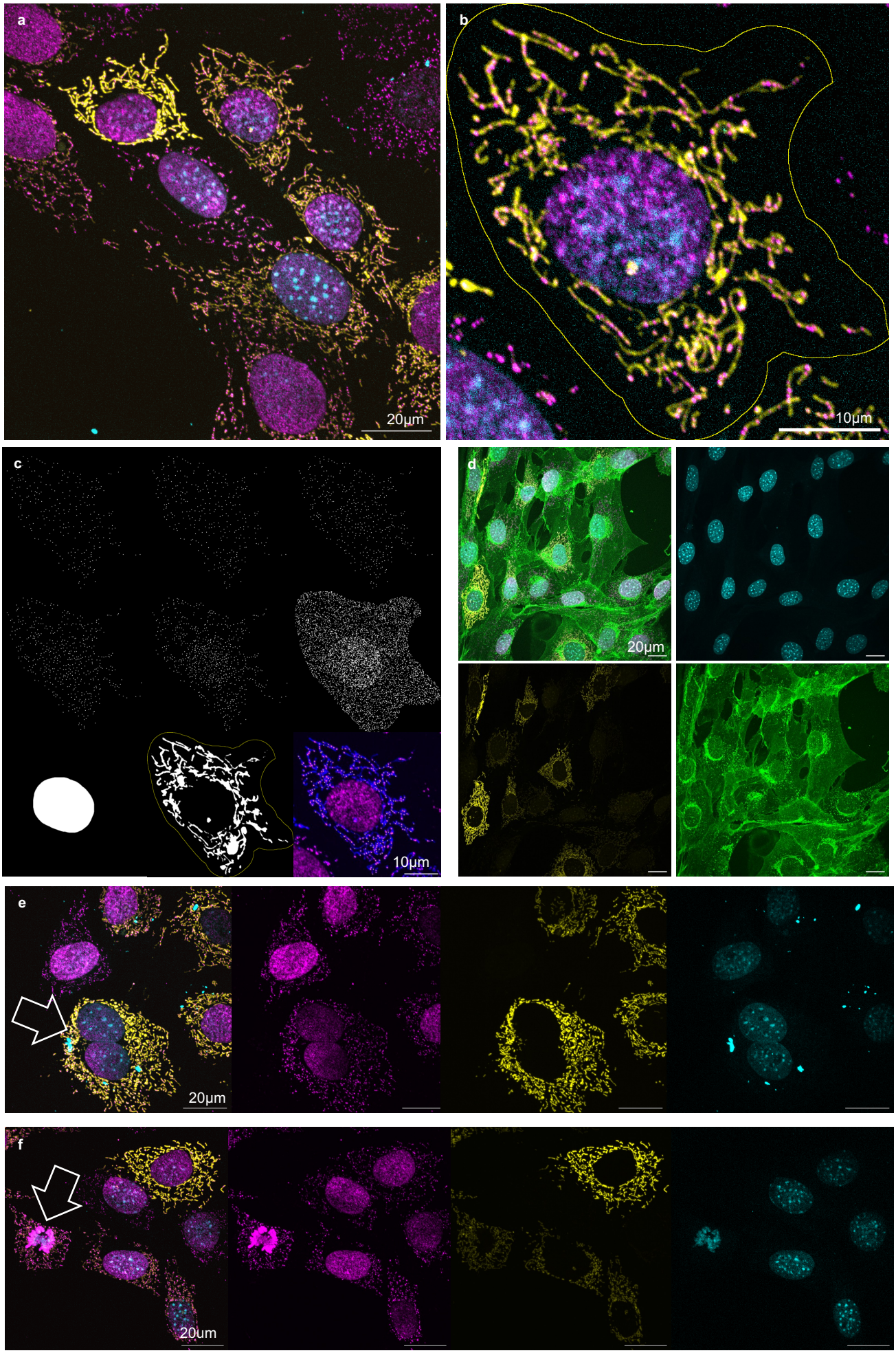

Supplementary Figure 2g

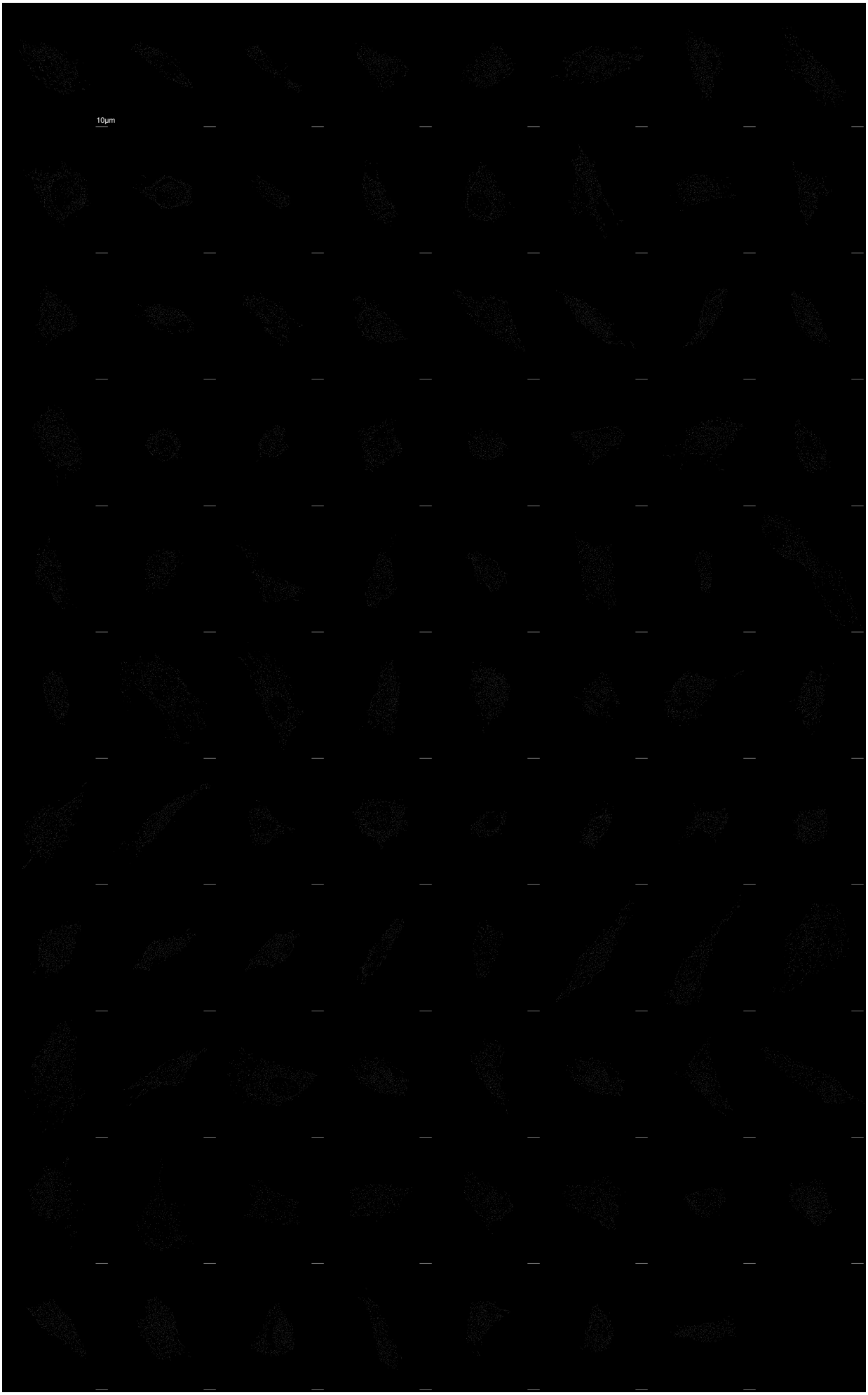

Supplementary Figure 2h

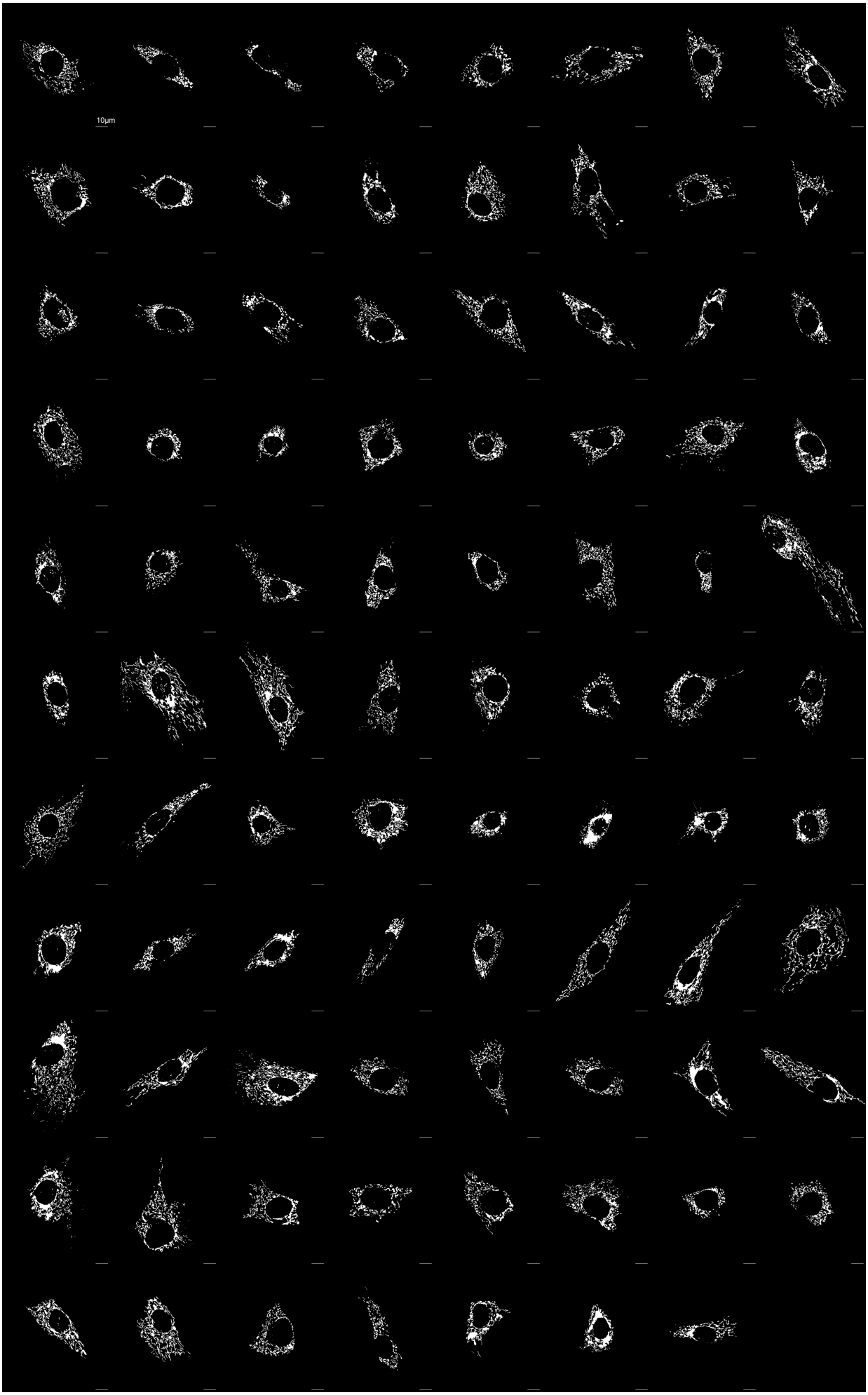

Supplementary Figure 2i

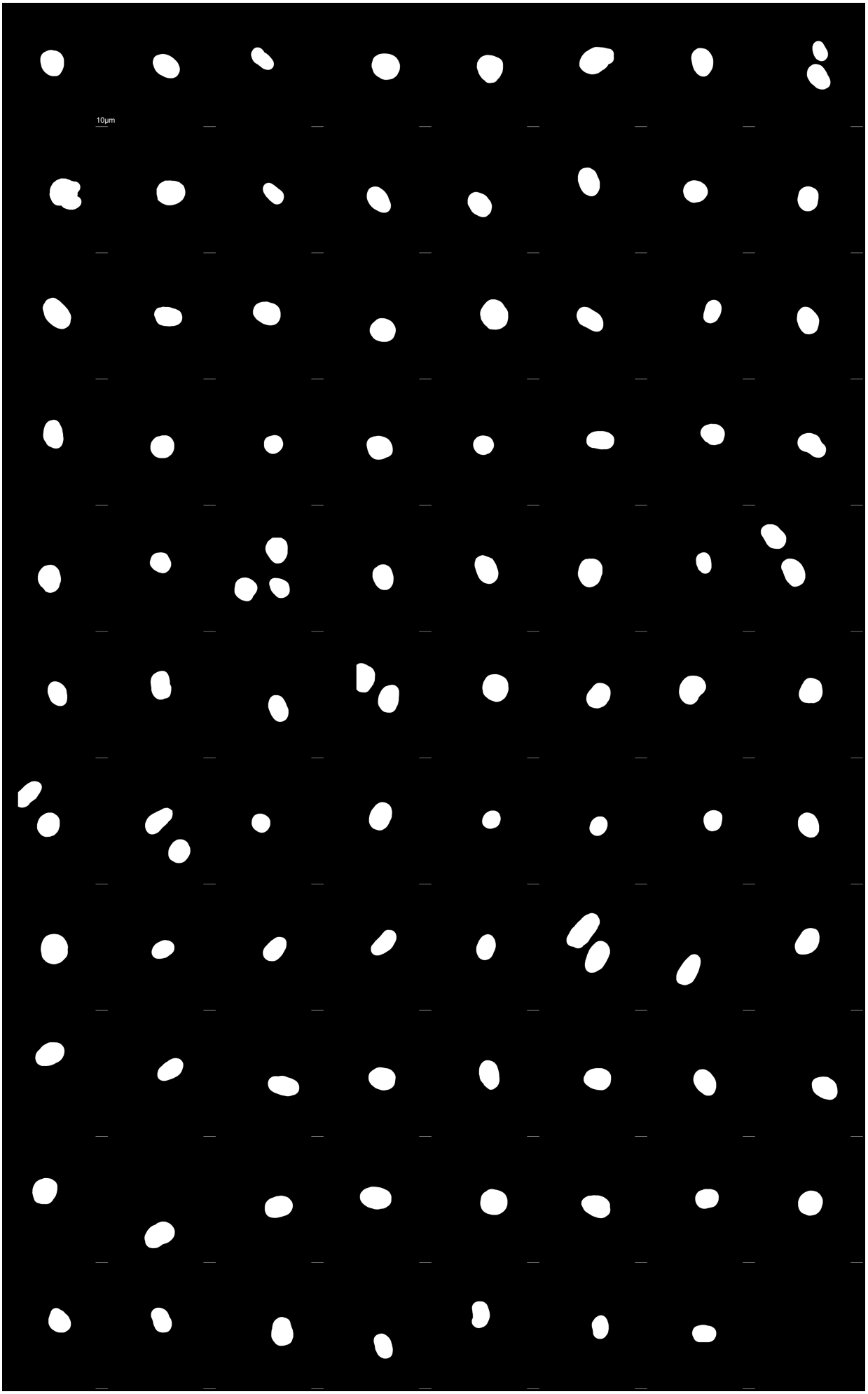

Supplementary Figure 3